Critical behavior of Mg_{1–x}Fe_{x}O at the pressure-induced iron spin-state crossover

K. Glazyrin, R. Sinmyo, E. Bykova, M. Bykov, V. Cerantola, M. Longo, C. McCammon, Vitali B. Prakapenka, and Leonid Dubrovinsky

Phys. Rev. B **95**, 214412 — Published 19 June 2017

DOI: 10.1103/PhysRevB.95.214412

Critical behavior of $Mg_{1-x}Fe_xO$ at the pressure induced iron spin state crossover.

K. Glazyrin[1], R. Sinmyo[2], E. Bykova[2], M. Bykov[2], V. Cerantola[2], M. Longo[2], C. McCammon[2], V. Prakapenka[3], Leonid Dubrovinsky[2]

[1] *FS-PE, Petra III, Deutsches Elektronen Synchrotron, 22607 Hamburg, Germany*

[2] *Bayerisches Geoinstitut, Universität Bayreuth, 95440 Bayreuth, Germany*

[3] *GeoSoilEnviroCARS, University of Chicago, Argonne National Laboratory, Argonne, IL 60439, USA*

I. ABSTRACT

We present a high-pressure study of $Mg_{1-x}Fe_xO$ (ferropericlase, Fp) single crystals $0.04(1)\leq x\leq 0.33(1)$ with a focus on ferrous iron spin-state crossover and the material behavior preceding it. Using Vegard's law and the most accurate high-pressure single crystal experimental data, we extract the lattice parameter a_{FeO}^{HS} of the "FeO high spin lattice contribution" in the MgO-FeO solid solution. We find that ferropericlases with a wide range of compositions share the same critical parameter a_C (defined as the minimum a_{FeO}^{HS} after which spin crossover starts). Furthermore, we discuss the effect of composition on spin crossover in ferrous iron in ferropericlase in the limits of low and moderate concentrations of Fe^{2+}.

II. INTRODUCTION

The behavior of ferropericlase ($Mg_{1-x}Fe_xO$, Fp) at high-pressure conditions plays a crucial role in our understanding of processes related to the interiors of the Earth and Earth-like rocky planets. Indeed, there is a significant amount of this mineral in the Earth's lower mantle, and we expect a plethora of complex physical phenomena related to the ferrous iron high spin – low spin (HS-LS) crossover [1], ranging from variation of elastic properties [2] to the redistribution of chemical elements between Earth's major lower mantle minerals [3]. This seemingly simple system has attracted more and more attention from the solid physics community due to the possibility of HS-LS crossover having a quantum critical nature [4].

There are numerous X-ray diffraction studies addressing the compression of Fp, many investigating the effect of pressure on the cubic unit cell and on the onset of the HS-LS transition [5–7]. However, most of the studies were conducted on powder material, where a strong discrepancy is observed even between results obtained on similar materials at seemly

the same hydrostatic conditions (e.g. [6–8]). As was discussed recently [8], the discrepancies may be related to effects of undesirable stress-strain relations (deviation from hydrostatic conditions) which evolve in powders on the macro- and microscale, even in pressure media offering optimum quasi-hydrostatic conditions. In addition, the spin-state crossover in Fp can be classified as gradual (e.g. [9]). However, the degree of spin-state crossover completion for powder material was never closely investigated. As suggested in [8], the strains on the microscopic level (e.g., due to high concentration of defects) are of great importance for ferrous iron spin-state crossover, particularly in terms of stress/strain distribution on the microscale and on the free energy of the system.

A single-crystal high-pressure study conducted on a small specimen in quasihydrostatic conditions should improve our understanding of the physics of the process. However, there are few single-crystal studies on Fp available and most of them either have no intrinsic information on pressure-density correlation [10,11] or have an insufficient number of points to provide conclusive evidence [12]. To the best of our knowledge, this study is the first on single crystal Fp covering a wide range of compositions at pressures close to the HS-LS crossover. Our results help to resolve some long-standing inconsistencies and contribute to the understanding of physical principles governing spin crossover in solid solutions.

Here we present an ambient temperature high-pressure X-ray diffraction study conducted on Fp single crystals of five different compositions and covering low ($x<5$mol%) as well as moderate concentrations of iron ($5<x<30$mol%). We compressed these materials up to 82 GPa (depending on composition) and observe a clear signature of HS-LS crossover. The MgO-FeO system is a good example of a solid solution at ambient conditions, and we apply the formalism of Vegard's law to our high-pressure data. Next, we test critical behavior [13,14] of Fp and of the corresponding FeO end-member component responsible for HS-LS crossover. We take a closer look at the effects of pressure and composition and suggest that a single critical parameter determines the onset of the HS-LS transition in the limits of low and moderate iron content. The simplicity of the system allows us to generalize our observations of MgO-FeO to the general case of solid solutions with ferrous iron impurity incorporated into an octahedral structural environment. Thus, we consider that our results and the approach used can be further employed for prediction of pressure-induced HS-LS crossover in a wider range of materials.

III.EXPERIMENTAL DETAILS AND METHODS

Fp material was synthesized under high-pressure and high-temperature conditions in a Kawai-type multi-anvil apparatus (press) [15] at Bayerisches Geoinstitut, Bayreuth. Fine grained MgO and Fe_2O_3 (95% enriched in ^{57}Fe) were first ground together for 1 hour. Mixtures were heated at 1473 K and 1 bar for 1 day in a CO-CO_2 gas-mixing furnace in which oxygen fugacity was controlled at $\log fO_2 = -11$ to reduce all Fe^{3+} to Fe^{2+}. Sample mixtures were loaded into metallic Re capsules and then packed into MgO containers. $LaCrO_3$ was used for the heater in the high-pressure assembly. The pressure and temperature used in the synthesis run was 14 GPa and 1873 K, respectively, with a heating duration of 20 min. After sample recovery from the Re capsule, the chemical compositions of the bulk synthesized material were analysed using electron microprobe analysis with a JEOL JXA-8200 instrument under the operating conditions of 15 kV and 15 nA where 20 points were collected for each set. The $Fe^{3+}/\Sigma Fe$ ratios of the synthesized samples were characterized by conventional Mössbauer spectroscopy using a constant acceleration Mössbauer spectrometer in transmission geometry equipped with a ^{57}Co source (Rh matrix). The velocity scale was calibrated using α-Fe foil. The Mössbauer spectra were analysed using the MossA software package [16] and Fityk [17]. While Mössbauer spectroscopy was essential for the characterization of the synthesized material, it is less important for our main discussion. We present a short description of the Mössbauer spectroscopy data in Supplementary materials [18]. The samples originating from the multianvil synthesis are labelled KNFp1, KNFp2, v4aFp1, and v4aFp4. The naming convention indicates the sample loadings, namely, the crystals KNFp1 and KNFp2 were placed into the cell 'KN', while v4aFp1 and v4aFp4 were placed into the cell 'v4a'. One additional sample batch with composition x=0.19(1) was produced by M. Longo using the procedure fully described in Ref. [19]. The sample b90Fp5 belongs to this batch.

Single crystals (with approximate lateral dimensions of 5-10 x 10-15 x 3-5 μm^3) were loaded into sample chambers of Mao-type symmetrical diamond anvil or BX90 cells (DACs) together with small ruby spheres (Rb) employed as pressure sensors. The crystals were either preselected by X-ray diffraction before the gas loading (b90Fp5) or tested with X-rays immediately after to optimize experimental time (KNFp1, KNFp2, v4aFp1, and v4aFp4). For the latter set, the initial selection, preceding the actual gas loading, included an inspection of the crystal shape (single grain vs multigrain) and optical clarity (absence of visible grain boundaries for transparent material with low concentration of iron). Thus, for the same set we could not measure the unit cell volumes at ambient conditions. The initial plan to determine

volume upon decompression was not possible due to the failure of diamond and gasket sample chamber.

The sample chambers inside rhenium gaskets were loaded with Ne pressure medium. The choice of a sample with small dimensions together with Ne pressure medium was important for maintaining experimental conditions close to hydrostatic. The equation of state for Ne [20] was used to cross check the consistency of pressures determined by Rb. The difference in pressures found from Ne and Rb markers were below 3 GPa at the highest pressures reached. Additional discussion on the hydrostatic conditions of the lower mantle and relevance of the sample state and size are given in the Supplementary materials.

For all samples with the exception of b90Fp5, X-ray diffraction patterns were obtained with a wavelength of 0.289Å at P02.2 (beamsize $3{\cdot}8um^2$), Extreme Conditions Beamline, Petra-III, DESY, Hamburg, Germany. The data on sample b90Fp5 were collected using a wavelength of 0.2952Å at IDD13 (beamsize $2.5{\cdot}4um^2$), GeoSoilEnviroCARS (GSECARS), APS, Argonne, USA. For each pressure point, X-ray diffraction data were collected on sample rotation (±32º, or ±38º ω rotation axis, depending on the DAC opening angle). The sample-detector distance was calibrated with a CeO_2 standard. Positions of diffracted peaks (6 to 9 unique reflections for each pressure point) were extracted using Fit2D [21] and used for calculation of lattice parameters employing Fityk/Unitcell software [17,22]. A single composition (b90Fp5) was analyzed with the Rigaku Crysalis PRO software package [23]. The values for the lattice parameters obtained using different software packages are consistent with one another.

Compositions of the individual crystals (multianvil synthesis samples KNFp1, KNFp2, v4aFp1, v4aFp4) were determined from the measured equation of state and the known variation of lattice parameters as a function of composition at ambient conditions [24,26]. The validity of the approach was additionally tested and confirmed using the well pre-characterized sample b90Fp5. For this sample, we compared values obtained with equations of state with ambient pressure data, and found good agreement within the experimental uncertainties (see below).

We use the information on the ambient pressure-volume value as a composition marker, since we cannot rely on information from the bulk synthesis. Indeed, during our experiments on the batch produced in the multianvil experiments, we confirmed the existence of magnesioferrite single crystals grown together with Fp. Additional discussion is presented in the Supplementary materials. The crystals used in this study had no parasitic diffraction that

could be attributed to magnesioferrite. The corresponding measurements are reported and described below.

IV. RESULTS AND DISCUSSION

A. Compressibility of Fp

The compression curves for the individual crystals are shown in Figure 1. From analysis of the data, we can sort compositions of the crystals by increasing concentration of iron in the following way: lowest Fe content - KNFp1 (blue square) and KNFp2 (red square), intermediate concentration - v4aFp1 (black triangle), b90Fp5 (inverse green triangle), and the highest concentration - v4aFp4 (circles). We observe no splitting of diffraction peaks up to the highest pressures, and conclude that the studied Fp material remains in the cubic (space group *Fm-3m*) NaCl B1-type structure at all pressures of our study.

We derive information on the elastic behavior of Fp in the HS state by fitting pressure (P) as a function of volume (V) using a 2nd order Birch-Murnaghan (BM) equation of state (EOS) [25]. Through this process, we obtain the following parameters: V_0 – unit cell volume, and $K_0=-V\cdot dP/dV|_{P=0GPa}$ – isothermal bulk modulus, both at ambient conditions. Following the definition of the employed EOS, the model has a fixed value of $K'=dK/dP=4$, the first pressure derivative of the isothermal bulk modulus (K). By knowing the volume or lattice parameters at ambient conditions, we can extract the composition of the material [24,26–28]. The corresponding parameters are listed in Table 1 (Supplementary materials) for the following iron compositions: $x=x_{Fe}$: x=0.04(1) (KNFp2), x=0.06(1) (KNFp1), x=0.09(3) (v4aFp1), x=0.19(1) (b90Fp5), and x=0.33(1) (v4aFp4). Figure 2 demonstrates that the obtained parameters, namely, x, K_0 and V_0, are in good agreement with the trend from literature data (references given in the figure caption).

The choice of EOS is additionally supported by a plot of normalized stress (F) as a function of Eulerian strain (f_E) (Figure 3). The F-f_E relation, commonly called a 'F-f plot', is a standard tool for analysis of high pressure P-V data. Additional information on the F-f plot and its relation to detection of spin state crossover in Fp and transitions in other materials can be found elsewhere [8,29–31].

Figure 3 highlights the closest experimental point to HS-LS crossover by means of large symbols with yellow background. X-ray diffraction data and F-f plots allow HS-LS crossover to be detected for iron concentrations at least as low as 4(1) mol% Fe, which corresponds to 4 ferrous ions per 25 unit cells of Fp in an ideal solid solution. Thus, X-ray diffraction is an

exceptionally sensitive tool to detect spin state transitions manifested through volume contraction.

First, we compare our P-V data with the primary pressure scale of MgO reported previously [32]. The latter study reports integration of MgO single crystal data from Brillouin scattering measurements and density data from polycrystalline X-ray diffraction with pressures below 55 GPa. We note that the ambient temperature BM or Vinet EOSs of MgO available in the literature or those employed here [32–36] are consistent with one another in the pressure range of interest [37] and that the choice of EOS does not change our results (see also Figure 2). In excellent agreement with previously published data [5–7,10,38], for pressures below the HS-LS crossover, the volumes of all Fp samples lie above the MgO compression line ("MGL" – MgO EOS line on Figure 1). Upon the further compression, the volumes of our single crystals drop significantly below the MGL after HS-LS crossover. This new observation stands out in strong contrast with all data previously published on powders, with the notable exception of data on Fp (x=0.17) [38] and Fp (x=0.1) [10]. Indeed, a careful examination shows that the Fp unit cell volume in these studies drops gradually below the MGL for pressures above the HS-LS crossover. Still, even in Refs [10,38], the effect of pressure on volume is not as profound as for our single crystal data.

This discrepancy in behavior may be related to differences in the initial state of sample material on the microscale. Following the recent discussion [8], if one compares compression of single crystals with powders we may expect additional strains or stresses due to grain-grain interactions which may (a) induce a metastable state, preventing a full transformation of ferrous iron into a ground LS state, and (b) result in a rhombohedral distortion of the system, presumably affecting the onset of spin crossover [8]. In addition, the grinding process, which is essential for powder preparation, should significantly increase the defect concentration in the grains, usually developing in the form of dislocations and, thus, induce additional micro-strain fields in the vicinity of Fe^{2+} ions. The influence of defects on electronic levels in Fp material was already suggested previously in a Mössbauer study [39] and may indeed contribute to the deviation from equilibrium upon HS-LS crossover. Along similar lines, the same microstrains and defects may lead to retention of a significant HS fraction, which is not surprising for systems with spin-state crossover [9]. To our knowledge, this effect was not taken into account in previous X-ray emission or Mössbauer (time or energy domain) spectroscopy studies due to low detection sensitivity.

In our single crystal study, we minimize the contribution from undesirable effects of grain boundaries, intergrain stresses, and grinding-induced defects, and thus transform the materials

to a configuration closer to thermodynamic equilibrium. We consider that our observations on the effect of mechanical treatment of the material on spin crossover deserve further exploration in future. As a final note, we found that the Fe^{2+} ionic radius in the LS state under high pressure becomes smaller than the radius of Mg^{2+}.

B. Application of Vegard's law to high-pressure data

We used the Vegard's law concept for analysis of the data describing the behavior of MgO-FeO solid solutions at high pressures. At ambient and high-pressure conditions the lattice parameter of $Mg_{1-x}Fe_xO$ can be described as a linear combination of the end-member lattice constants. Knowing the MgO equation of state, we can write the following relations:

$$a_{Fp} = a_{MgO} \cdot (1 - x) + a_{FeO}^{HS/LS} \cdot x;\ a_{FeO}^{HS/LS} = (a_{Fp} + a_{MgO} \cdot (x - 1))/x, \qquad (1)$$

where a_{Fp}, a_{MgO} and $a_{FeO}^{HS/LS}$ are the isothermal pressure dependent lattice parameters of Fp with composition $Mg_{1-x}Fe_xO$, MgO, and FeO, respectively. The parameter $a_{FeO}^{HS/LS}$ is related to FeO and describes its respective contribution to the Fp phase for the HS state (a_{FeO}^{HS}), LS state (a_{FeO}^{LS}) or for a combination of states ($a_{FeO}^{HS/LS}$). The results of our analysis are shown in Figure 4. As in Figure 3, the large symbols with yellow background indicate points closest to the beginning of spin-state crossover.

The distinctive behavior of the $a_{FeO}^{HS} = f(P)$ slope allows us to identify two groups of samples (Figure 4). The first CLASS-1 (blue line) includes only one sample KNFp2 with composition x=0.04(1). The second, CLASS-2 (black line), encompasses KNFp1, v4aFp1, b90Fp5, v4aFp4, and, thus, corresponds to the range $0.06(1) \leq x \leq 0.33(1)$. The averaged slope for these studied compositions is estimated as $-6.4(5) \cdot 10^{-3}$ Å/GPa. The table and a figure with slopes for all studied samples are provided in Supplementary materials. We note that a small variation in composition (x=0.04 → x=0.06) produces a major effect, separating KNFp1 and KNFp2 in particular, corresponding to CLASS-1 and CLASS-2, respectively. Further discussion on CLASS-1 and CLASS-2 is presented following additional evidence that they are indeed different.

In Figure 4, the value $a_C = a_{FeO}^{HS}$ is introduced as a special critical parameter corresponding to the smallest value of a_{FeO}^{HS} such that further compression starts the transformation of ferrous iron to the LS state. This behavior is highlighted by horizontal dashed lines. Again, the same

apparent difference in CLASSs 1 and 2 are seen which is additionally illustrated by analysis of the corresponding a_C values, shown in the inset of Figure 4.

CLASS-1 corresponds to Fp with a low concentration of iron, with tentative boundary for *x* between 0.04(1) and 0.06(1). We hypothesize that for solid solutions with substantially low concentration of iron atoms, the Mg environment (i.e., absence of significant interference between Fe^{2+} ions) determines the onset of the HS-LS transition. It is obvious that compression of iron and its electrons in the octahedral "cage" made of oxygen can be expressed by the lattice parameter a_{Fp} or the parameter a_{FeO}^{HS} introduced above. The variation of the a_{FeO}^{HS} slope for CLASS-1 as a function of the actual composition may require additional investigation.

Fp compositions with low to moderate concentration of iron $x \geq 0.06(1)$ belong to CLASS-2. These compositions are indeed interesting for geophysics and mineral physics, as they are expected to occur in the Earth's mantle and other planetary interiors. Our observation that a_{FeO}^{HS} for CLASS-2 samples is nearly invariant with pressure will be useful for future simulations of compression behavior of virtually any relevant Fp phase in the HS state. We envisage an extension of our analysis and application to the high temperature limit of Fp in the HS state, and thus to simulations of actual conditions in the lower mantle. Isobaric heating should increase the overall lattice parameters of Fp, and, thus - a_{FeO}^{HS}, making LS less favorable. Our reasoning is consistent with experimental observations of a positive Clausius-Clapeyron slope for HS-LS crossover for Fp with x=0.25 [4,40].

After analyzing available data for Fp with different compositions, it is clear that at x>0.04(1), the influence of Mg NNN on HS-LS crossover in iron decreases. This observation is consistent with statements in the literature that, on the microscale, Fp is not an ideal solid solution and that Fe exhibits clusterization [41]. The introduction of Fe-Fe interaction can indeed explain the similar slope of $a_{FeO}^{HS} = f(P)$ and the similar value of $a_C = 4.014(5)$Å for all Fp that belong to CLASS-2.

The universality of a_C is demonstrated through comparison with Fp data from Mao et al. with x=0.25 [40]. Their powder sample with composition in the vicinity to the one expected for the Earth's lower mantle was surrounded by a solid pressure medium (KCl) and was laser annealed prior to collection of ambient temperature data to release stress. According to existing capability at the time, the laser annealing would have removed undesirable stress to a certain degree. As discussed previously [8], the results of [40] are in better agreement with

other experimental reports than the study of Fei et al. [5], for example. From the composition, our b90Fp5 sample is very close to that investigated by Mao et al. [40].

Comparing our data with those from Ref [40] (grey circles with an embedded star, Figure 4), we highlight similarities in slope for α_{FeO}^{HS} below ~35 GPa with the characteristic trend of CLASS-2 materials (thick black line on Figure 4). The small differences between the trends above 35 GPa can be attributed to various effects, for example non-hydrostatic conditions or insufficient annealing duration. As further support of this hypothesis we note that the deviation becomes larger with increasing compression. We also note the strong deviation from the trend of our Fp sample containing a higher concentration of iron, i.e., v4aFp4, x=0.33(1). Even so, the critical value of α_C in the powder sample of [40] is almost the same as for the single crystals in CLASS-2 that we studied.

C. HS-LS crossover and the critical phenomena approach

In the previous section, we defined the parameter α_{FeO}^{HS} and determined its critical value α_C below which HS-LS crossover starts. We now follow an approach similar to the theory of critical phenomena to investigate the behavior of $\alpha_{FeO}^{HS/LS}$ in the vicinity of the critical pressure P_C (Figure 5). The typical methodology in the theory of phase transitions and critical phenomena investigates various properties, for example order parameters, universality, scaling and normalization [14]. However, as previously discussed in the literature [13,42], it is equally important to study properties of practical importance such as heat capacity, lattice parameter(s) and so on in the vicinity of the phase transition. We investigate $\alpha_{FeO}^{HS/LS}$ in the vicinity of the critical pressure P_C corresponding to the point with $\alpha_{FeO}^{HS/LS} = \alpha_C$.

Initially there appears to be no clear correlation between pressure and $\alpha_{FeO}^{HS/LS}$. However, the correlation becomes evident if we calculate the differences $\alpha_C - \alpha_{FeO}^{HS/LS}$ and $P_C - P$ and plot them on a logarithmic scale (Figure 5). The model of critical exponent $(\alpha_C - \alpha_{FeO}^{HS/LS}) \sim (P_C - P)^{\gamma}$ describes our data well for all crystals, where the corresponding values of γ are given in the inset to Figure 5. Analysis of the data shown in the inset shows that the value of the critical exponent γ is correlated with iron concentration.

A simple fit to the function $\gamma = A \cdot ArcTan(B \cdot x)$, with A= 0.717(2) and B=27.57(24), shows surprising agreement with our data (excluding the b90Fp5 data points) (Figure 5).

However, we note the sensitivity of γ to the selection of P_c. For example, the olive and light green points shown in Figure 5 refer to the same sample (b90Fp5) assuming P_c values of 53.2 GPa (as determined from Figure 3, the large inverse green triangle with yellow background) and 50 GPa, respectively. Thus, further experiments with finer pressure steps around spin crossover may be required for more accurate determination of critical parameters and detailed insight into their nature.

D. Low concentration limit

The origin of the different behavior of Fp CLASS-1 and CLASS-2 can be further investigated following an approach suggested by Kantor et al. [41]. For the NaCl-type (B1) crystal structure of Fp, each cation (Mg or Fe) has 12 next-nearest cation neighbors (NNN). We can define the partial probability $P(n, P_{Fe-Fe})$ of the central Fe atom to have *n* cations of Fe in its NNN coordination shell through the known pair correlation function P_{Fe-Fe}:

$$P(n, P_{Fe-Fe}) = P_{Fe-Fe}^{n}(1 - P_{Fe-Fe})^{12-n}\frac{12!}{n!\,(12-n)!}$$

Note that for a single atom, the total probability to have a neighbor $(\sum_n P(n, P_{Fe-Fe}))$ is a sum of individual contributions from $P(1, P_{Fe-Fe})$, $P(2, P_{Fe-Fe})$ and etc.

Based on the assumption that $P_{Fe-Fe} = x = x_{Fe}$ for an ideal solid solution with a fully random distribution of Fe, we can determine $P(1) = P(1, x_{Fe})$ (Figure 6), which is the probability to have a single atom of Fe in the NNN shell. At the same figure, we also demonstrate $P(2)$ and $P(3)$. This functional form corresponds to the competition between Fe and Mg cations around the central Fe atom, and thus the Fe-Fe correlations. $P(1)$ function is highly asymmetric with a steep slope at values of x_{Fe}<0.05. For illustration, the compositional uncertainties for KNFp1 and KNFp2 are overlaid with $P(1, x_{Fe})$ in Figure 6. Indeed, a small shift of x_{Fe} from KNFp1 (red) to KNFp2 (blue) should lead to a large change of $P(1, x_{Fe})$, which in terms of total probability should be the dominating contribution from other $P(n, x_{Fe})$ in the limit of the very low doping concentration. Any increase of concentration boosts the contribution from the functions of higher order, i.e. $P(2, x_{Fe-Fe})$, $P(3, x_{Fe-Fe})$, etc. Thus, a reasonably small change in concentration can lead to strong variations of total

probability, and the steepness of the $\sum_n P(n, P_{Fe-Fe})$ slope together with diminishing role of $P(n, x_{Fe-Fe})$ ($n>1$) can indeed explain the difference between CLASS-1 and CLASS-2. Our study provides experimental evidence that illustrates the importance and the effect of the Fe-Fe correlation for low impurity concentrations in solid solutions.

V. Conclusion

In summary, we present a high-pressure single-crystal X-ray diffraction study of $Mg_{1-x}Fe_xO$ with a wide range of compositions $0.04(1) \leq x \leq 0.33(1)$ and describe its compression under quasi-hydrostatic conditions. Our observations allow two different classes for MgO-FeO solid solutions to be identified based on their compressional behavior for low concentrations of impurity elements (CLASS-1, $x<0.06(1)$) and moderate ones (CLASS-2, $x\geq0.06(1)$). We suggest an explanation for the different behavior of CLASS-1 and CLASS-2 by analyzing the probability of Fe-Fe correlations in a simple next-nearest neighbor model.

Using Vegard's law we analyze high-pressure data and extract the lattice parameter contribution $a_{FeO}^{HS/LS}$ of the "FeO-component" in MgO-FeO solid solution. In our experiments, we isolate the parameter a_C as a minimum value of a_{FeO}^{HS}, such that higher compression triggers the spin crossover of ferrous iron. We find that CLASS-2 ferropericlase shares the same critical parameter a_C over a wide composition range within the uncertainty of experiments.

Our observations are equally important for the geophysics, mineral physics, and materials physics communities. Indeed, we report clear regularities in the behavior of MgO-FeO solid solutions with composition range relevant for planetary science and with a focus on pressure-induced spin crossover. Our observations may also be applicable to a larger class of compounds with ferrous iron occupying an octahedral oxygen environment. Moreover, our results indicate that knowledge of end-member compression behavior may allow prediction of the spin-crossover conditions and basic description of corresponding material transformation for a wide class of materials containing transition metal elements.

VI. Figures

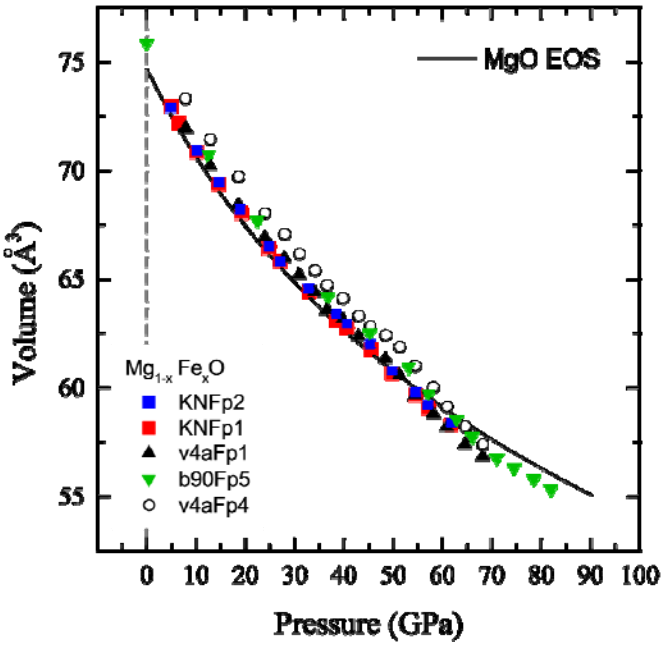

Figure 1

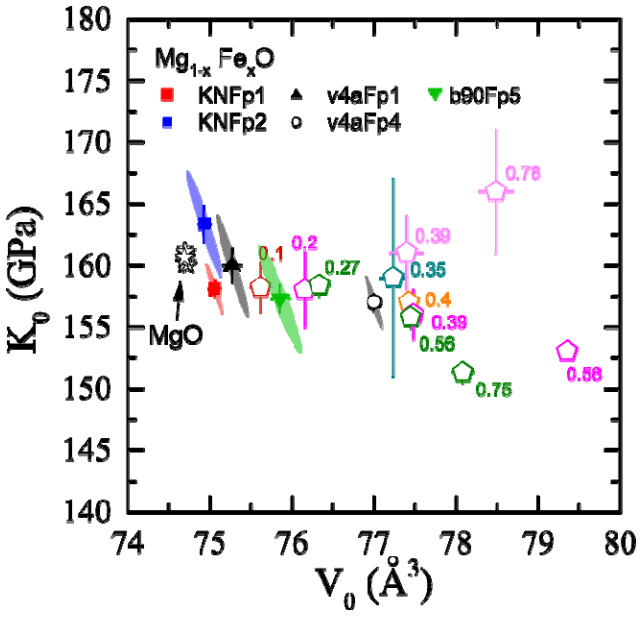

Figure 2

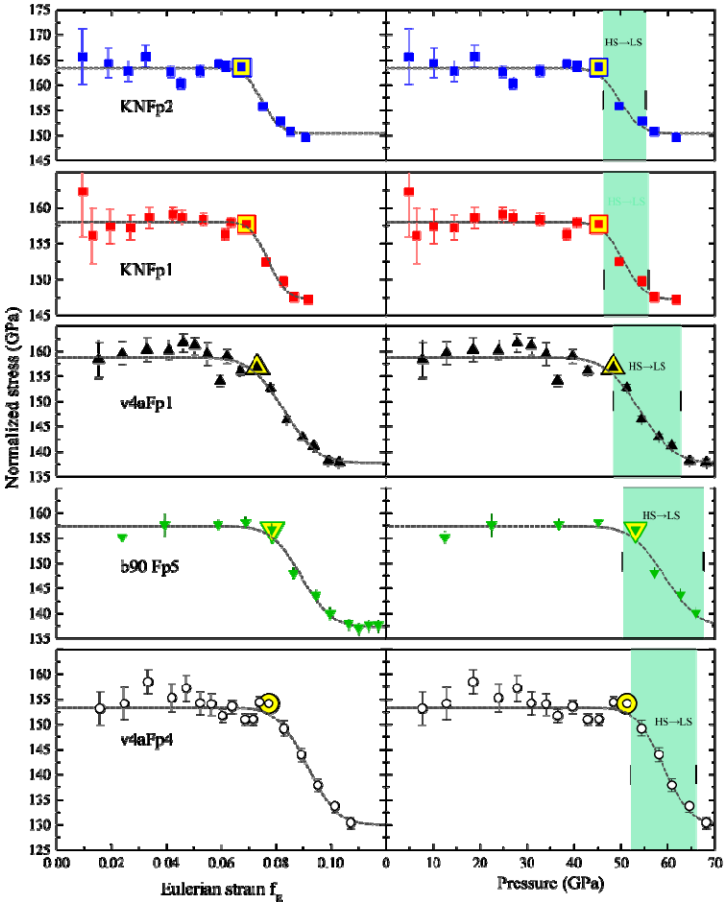

Figure 3

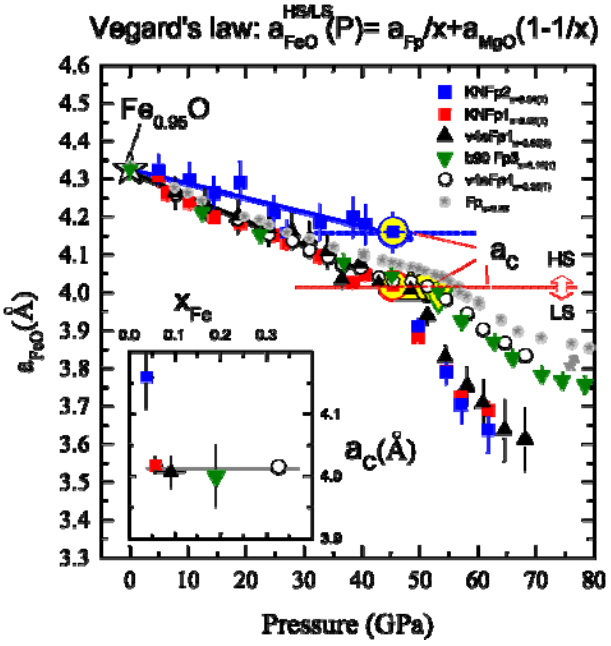

Figure 4

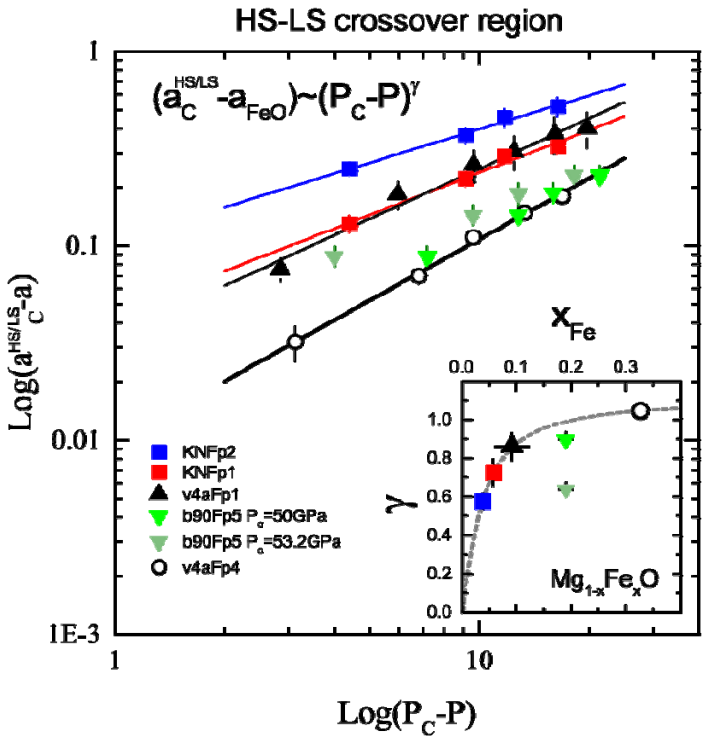

Figure 5

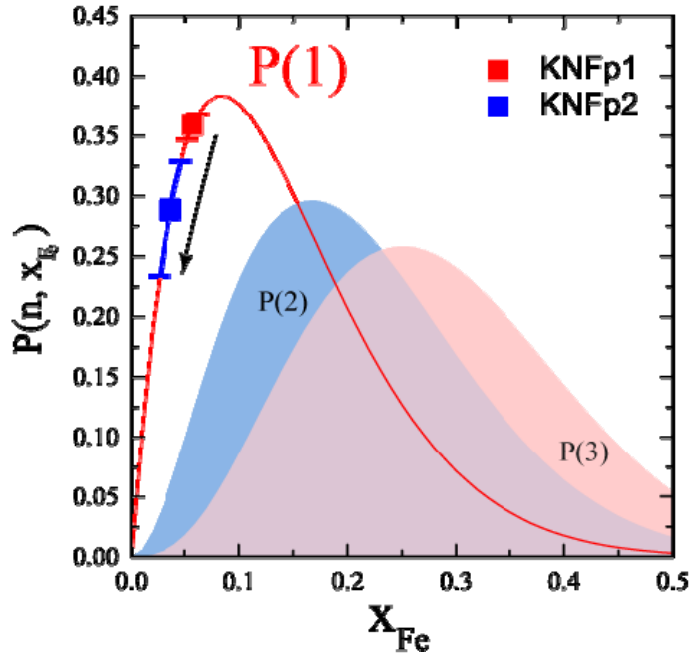

Figure 6

VII. Figure Captions

Figure 1 (color online only) Unit cell volume of individual single crystals as a function of pressure. Note the compositional difference of crystals reflected through the different unit cell volumes at a given pressure and a different magnitude of volume contraction at the HS-LS crossover. Sample labels in the legend are sorted according to increasing iron concentration from top to bottom.

Figure 2 (color online only) Variation of Fp isothermal bulk modulus K_0 with V_0 for various $Mg_{1-x}Fe_xO$ iron concentrations (HS state). Our data points (red, blue squares; black triangle, open circle) are shown together with the corresponding equation of state fit covariance ellipses. All other points correspond to literature data, and they are indicated with pentagons (Fp) and star symbols (MgO) together with labels indicating published iron concentrations. The MgO data points represent published data and cover both Birch-Murnaghan (BM) [32–35] and Vinet [36] equations of state. Fp data points include the following data: orange [43], green [26], magenta [5], dark red [10], pink [6], and cyan [7]. Most of the Fp literature data were described with the BM equation (K'~4) with the exception of the green points which correspond to K'~5.5. The reported error bars for literature data are shown in the figure if available.

Figure 3 (color online only) Normalized stress (F) as a function of Eulerian strain (f_E) and pressure reported for the studied compositions. Large symbols with yellow background indicate the last experimental pressure points with Fp in a presumably pure HS state. The green region emphasizes the spin-crossover pressures. As expected [2,8], the crossover region shifts towards higher pressures with composition. The wider crossover region for the bx90Fp5 can be attributed to the lower density of the experimental points.

Figure 4 (color online only) Variation of $a_{FeO}^{HS/LS}$ as a function of pressure. Note the slope induced by compression for Fp in HS state. We observe similar behavior (thick black solid line) for KNFp1 - x_{Fe}=0.06(1), v4aFp1 - x_{Fe}=0.09(2), and v4aFp4 - x_{Fe}=0.33(1) and a distinct one (solid blue line) for KNFp2 - x_{Fe}=0.04(1). Large open symbols indicate a_c – critical values of $a_{FeO}^{HS/LS}$. Compression leads to smaller values of $a_{FeO}^{HS/LS}$, and the values lower than a_c correspond to the onset of HS-LS crossover (indicated by the red dashed line). We highlight

the similar values of a_C for a wide range of Fp compositions above x_{Fe}>0.06(1) for our data and those from the literature with a gray line. The large open star symbol at 0 GPa corresponds to the reference $Fe_{0.95}O$ lattice constant (NaCl B1-type structure) measured at ambient conditions, basically coinciding with the ambient values $a_{FeO}^{HS}|_{P=0Gpa}$ exhibited by the trend of the studied $Mg_{1-x}Fe_xO$ compositions. Gray circles with a white star represent data from similar material [40], x_{Fe}=0.25 (sample in KCl pressure medium, laser annealing). The double-sided gray arrow highlights the discrepancy of our data with literature values (see main text for discussion). The inset demonstrates the variation of a_C as a function of iron concentration.

Figure 5 (color online only) Relative change of $a_{FeO}^{HS/LS}$ as a function of relative pressure within the spin crossover region. Parameters indicating the reference critical pressure P_C and the critical FeO lattice contribution a_C are introduced in the text. We use decimal logarithmic scale for the pressure range of the crossover. The parameter γ can be estimated from the slope of the linear dependency shown in the Figure and the result of the fit is shown by means of solid lines. We indicate a possible correlation with an eye guide (gray dashed line) and present additional discussion in the main text.

Figure 6 (color online only) Partial probability $P(n, x_{Fe})$ for Fe (n=1, 2, 3) to occupy the NNN shell of a cation as a function of the impurity element concentration $x = x_{Fe}$ for the Fp crystal structure. Note that the total probability ($\sum_n P(n, x_{Fe})$) for an Mg/Fe atom to have a nearest neighbor is a sum of individual contributions. It is clear that $P(1, x_{Fe})$ becomes the dominating factor at values of x<0.05. Compositions corresponding to KNFp1 and KNFp2 are indicated. We emphasize the curvature of $P(1, x_{Fe})$ and its slope steepness at low x_{Fe} values. For the change in composition from KNFp1 to KNFp2 illustrated by the arrow, the rapidly changing slope for total probability $\sum_n P(n, x_{Fe})$ may explain our observations of CLASS-1 and CLASS-2. It may explain the corresponding differentiation in the framework of the Fe-Fe correlation strength, i.e. the Fe-Fe correlations become weaker at lower x_{Fe} values.

VIII. References

[1] J. Badro, G. Fiquet, F. Guyot, J.-P. Rueff, V. V. Struzhkin, G. Vankó, and G. Monaco, Science (80). **300**, 789 (2003).

[2] J.-F. Lin, S. Speziale, Z. Mao, and H. Marquardt, Rev. Geophys. **51**, 244 (2013).

[3] T. Irifune, T. Shinmei, C. A. McCammon, N. Miyajima, D. C. Rubie, and D. J. Frost, Science (80). **327**, 193 (2009).

[4] I. S. Lyubutin, V. V Struzhkin, A. A. Mironovich, A. G. Gavriliuk, P. G. Naumov, J.-F. Lin, S. G. Ovchinnikov, S. Sinogeikin, P. Chow, Y. Xiao, and R. J. Hemley, Proc. Natl. Acad. Sci. U. S. A. **110**, 7142 (2013).

[5] Y. Fei, L. Zhang, A. Corgne, H. Watson, A. Ricolleau, Y. Meng, and V. Prakapenka, Geophys. Res. Lett. **34**, (2007).

[6] K. K. Zhuravlev, J. M. Jackson, A. S. Wolf, J. K. Wicks, J. Yan, and S. M. Clark, Phys. Chem. Miner. **37**, 465 (2009).

[7] B. Chen, J. M. Jackson, W. Sturhahn, D. Zhang, J. Zhao, J. K. Wicks, and C. a. Murphy, J. Geophys. Res. **117**, B08208 (2012).

[8] K. Glazyrin, N. Miyajima, J. S. Smith, and K. K. M. Lee, J. Geophys. Res. Solid Earth **121**, 3377 (2016).

[9] P. Gütlich, P. J. van Koningsbruggen Koningsbruggen, and F. Renz, *Recent Advances in Spin Crossover Research in Structure and Bonding* (Springer Berlin Heidelberg, 2004), pp. 27–75.

[10] H. Marquardt, S. Speziale, H. J. Reichmann, D. J. Frost, and F. R. Schilling, Earth Planet. Sci. Lett. **287**, 345 (2009).

[11] J. C. Crowhurst, J. M. Brown, a F. Goncharov, and S. D. Jacobsen, Science **319**, 451 (2008).

[12] D. Antonangeli, J. Siebert, C. M. Aracne, D. L. Farber, A. Bosak, M. Hoesch, M. Krisch, F. J. Ryerson, G. Fiquet, and J. Badro, Science (80-.). **331**, 64 (2011).

[13] H. Stanley, Rev. Mod. Phys. **71**, S358 (1999).

[14] H. E. Stanley, *Introduction to Phase Transitions and Critical Phenomena (International Series of Monographs on Physics)* (Oxford University Press, Oxford, UK, 1987).

[15] H. Keppler and D. J. Frost, EMU Notes Vol. 7 1 (2005).

[16] C. Prescher, C. McCammon, and L. Dubrovinsky, J. Appl. Crystallogr. **45**, 329 (2012).

[17] M. Wojdyr, J. Appl. Crystallogr. **43**, 1126 (2010).

[18] See Supplemental Material at [URL] for additional supporting information and discussions

[19] M. Longo, C. a. McCammon, and S. D. Jacobsen, Contrib. to Mineral. Petrol. **162**, 1249 (2011).

[20] Y. Fei, A. Ricolleau, M. Frank, K. Mibe, G. Shen, and V. Prakapenka, Proc. Natl. Acad. Sci. **104**, 9182 (2007).

[21] A. P. Hammersley, ESRF Intern. Rep. **ESRF97HA02**, (1997).

[22] T. J. B. Holland and S. A. T. Redfern, Miner. Mag **61**, 65 (1997).

[23] Rigaku Oxford Diffraction., (2014).

[24] B. Simons, Carnegie Inst. Wash. Yearb **79**, 376 (1980).

[25] F. Birch, Phys. Rev. **71**, 809 (1947).

[26] S. D. Jacobsen, H.-J. Reichmann, H. A. Spetzler, S. J. Mackwell, J. R. Smyth, R. J. Angel, and C. A. McCammon, J. Geophys. Res. **107**, 14 PP. (2002).

[27] Y. Fei, H. Mao, J. Shu, and J. Hu, Phys. Chem. Miner. **18**, (1992).

[28] R. H. Nafziger and A. Muan, Am. Mineral. **52**, 1364 (1967).

[29] F. Birch, J. Geophys. Res. **83**, 1257 (1978).

[30] B. J. Maier, A.-M. Welsch, B. Mihailova, R. J. Angel, J. Zhao, C. Paulmann, J. M. Engel, W. G. Marshall, M. Gospodinov, D. Petrova, and U. Bismayer, Phys. Rev. B **83**, 134106 (2011).

[31] R. J. Angel, in *High-Temperature Highpressure Cryst. Chem. MSA; Rev. Mineral. Geochemistry; Vol. 41*, edited by R. M. Hazen and R. T. Downs (2000), pp. 35–60.

[32] C. S. Zha, H. Mao, and R. J. Hemley, Proc. Natl. Acad. Sci. U. S. A. **97**, 13494 (2000).

[33] S. V Sinogeikin and J. D. Bass, Phys. Earth Planet. Inter. **120**, 43 (2000).

[34] S. Speziale, C.-S. Zha, T. S. Duffy, R. J. Hemley, and H. Mao, J. Geophys. Res. **106**, 515 (2001).

[35] Y. Fei, D. J. Frost, H.-K. Mao, C. T. Prewitt, and D. Häusermann, Am. Mineral. **84**, 203 (1999).

[36] A. Dewaele, G. Fiquet, D. Andrault, and D. Hausermann, J. Geophys. Res. **105**, 2869 (2000).

[37] K. Jin, X. Li, Q. Wu, H. Geng, L. Cai, X. Zhou, and F. Jing, J. Appl. Phys. **107**, 113518 (2010).

[38] J.-F. Lin, V. V. Struzhkin, S. D. Jacobsen, M. Y. Hu, P. Chow, J. Kung, H. Liu, H.-K. Mao, and R. J. Hemley, Nature **436**, 377 (2005).

[39] C. McCammon, J. Peyronneau, and J.-P. Poirier, Geophys. Res. Lett. **25**, 1589 (1998).

[40] Z. Mao, J.-F. Lin, J. Liu, and V. B. Prakapenka, Geophys. Res. Lett. **38**, L23308 (2011).

[41] I. Kantor, L. Dubrovinsky, C. McCammon, G. Steinle-Neumann, A. Kantor, N. Skorodumova, S. Pascarelli, and G. Aquilanti, Phys. Rev. B **80**, 14204 (2009).

[42] I. Herbut, *A Modern Approach to Critical Phenomena: Igor Herbut: 9780521142380: Amazon.com: Books* (Cambridge University Press, Cambridge, UK, 2010).

[43] M. Rosenhauer, M. H.-K., and E. Woermann, Carnegie Inst Washingt. Yearb. **75**, 513 (1976).